

A 250 GHz Survey of High Redshift QSOs from the Sloan Digital Sky Survey

C. L. Carilli¹, F. Bertoldi², M.P. Rupen¹, Xiaohui Fan^{3,5}, Michael A. Strauss³, K.M.

Menten², E. Kreysa², Donald P. Schneider⁴, A. Bertarini², M.S. Yun¹, R. Zylka²

¹National Radio Astronomy Observatory, P.O. Box O, Socorro, NM 87801, USA

²Max-Planck-Institut für Radioastronomie, Auf dem Hügel 69, D-53121 Bonn, Germany

³Princeton University Observatory, Peyton Hall, Princeton, NJ 08544, USA

⁴Dept. of Astronomy, Pennsylvania State University, University Park, PA 16802, USA

⁵Institute for Advanced Study, Olden Lane, Princeton, NJ 08540, USA

ccarilli@nrao.edu

Received _____; accepted _____

to appear in the *Astrophysical Journal* 2001

ABSTRACT

We present observations at 250 GHz (1.2 mm), 43 GHz, and 1.4 GHz of a sample of 41 QSOs at $z > 3.7$ found in the Sloan Digital Sky Survey. We detect 16 sources with a 250 GHz flux density greater than 1.4 mJy. The combination of centimeter and millimeter wavelength observations indicates that the 250 GHz emission is most likely thermal dust emission. Assuming a dust temperature of 50 K, the implied dust masses for the 16 detected sources are in the range 1.5 to $5.9 \times 10^8 M_{\odot}$, and the dust emitting regions are likely to be larger than 1 kpc in extent. The radio-through-optical spectral energy distributions for these sources are within the broad range defined by lower redshift, lower optical luminosity QSOs. We consider possible dust heating mechanisms, including UV emission from the active nucleus (AGN) and a starburst concurrent with the AGN, with implied star formation rates between 500 and $2000 M_{\odot}$ year $^{-1}$.

Subject headings: dust: galaxies — radio continuum: galaxies — infrared: galaxies — galaxies: starburst, evolution, active

1. Introduction

The existence of massive black holes at the centers of galaxies has long been predicated on consideration of the energetics of active galactic nuclei (AGN): accretion of matter onto a massive black hole is an order of magnitude more efficient at converting mass into energy than is stellar nucleosynthesis (Begelman, Blandford, & Rees 1984). The last few years have seen an explosion of dynamical evidence for massive black holes at the center of galaxies, and in the direct measurement of black hole masses from the dynamics of circumnuclear regions (Richstone et al. 1998; Miyoshi et al. 1996; Ghez et al. 1998; Genzel et al. 2000; Tanaka et al. 1995). These observations indicate that the overwhelming majority of spheroidal galaxies in the nearby universe contain massive black holes (Kormendy 2000). Moreover, a clear correlation has been found between the black hole mass and the velocity dispersion of the stars in the spheroid (Gebhardt et al. 2000, Ferrarese & Merritt 2000). This remarkably tight correlation suggests a ‘causal connection between the formation and evolution of the black hole and the bulge’ (Gebhardt et al. 2000; Kormendy 2000; Richstone et al. 1998).

Support for this general idea comes from: (i) the observed space density of high redshift Quasi-Stellar Objects (QSOs), which would require a massive black hole in most low z spheroidal galaxies (Kormendy & Ho 2000), (ii) the observation of similar rapid increases in the space densities of AGN and starburst galaxies from $z = 0$ to $z = 2$ (Boyle & Terlevich 1998, Blain et al. 1999), and (iii) the observation of co-eval AGN and star formation activity in some nearby nuclear starburst galaxies (Rigopoulou et al. 1999; Carilli, Wrobel, & Ulvestad 1999). On the other hand, the QSO population shows an abrupt turn-over in the co-moving number density at $z \geq 3$ (Schmidt, Schneider, & Gunn 1995a; Kennefick, Djorgovski, & de Carvalho 1995; Fan et al. 2001b). It is unclear whether such a turnover exists in the starburst population (Blain et al. 1999, Dunlop 2000). Also, questions remain

about the relative timescales for the commencement and duration of the starburst and AGN processes (Sanders & Mirabel 1996), and the origin at very high redshift of the ‘seed’ black hole (Richstone et al. 1998).

A particularly intriguing observation that has fueled the debate over co-eval starbursts and AGN at high redshift is the recent detection at 250 GHz of copious thermal dust emission from high redshift QSOs by Omont et al. (1996a). Omont et al. observed a sample of $z > 4$ QSOs from the Automatic Plate Measuring (APM) survey and found that 6 of 16 sources show dust emission with 250 GHz flux densities of 3 mJy or greater, with implied Far Infrared (FIR) luminosities, $L_{\text{FIR}} > 10^{12} L_{\odot}$, and dust masses $\geq 10^8 M_{\odot}$. Follow-up observations of three of these dust-emitting QSOs revealed CO emission as well, with implied molecular gas masses \approx few $10^{10} M_{\odot}$ (Guilloteau et al. 1997, 1999; Ohta et al. 1996; Omont et al. 1996b; Carilli, Menten, & Yun 1999).

Two different mechanisms have been proposed for heating the dust in high redshift QSOs. Given the large dust and gas masses, Omont et al. (1996a) make the circumstantial argument that star formation is inevitable, and hence that the dominant dust heating mechanism may be star formation. Supporting evidence comes from deep radio observations at 1.4 GHz, which show that the ratio of the radio continuum to submillimeter continuum luminosity from some of these sources is consistent with the well established radio-to-far IR correlation for low redshift star forming galaxies (Yun et al. 2000). And Omont et al. (2001) make the simple point that copious star formation is required in order to produce the dust. The implied star formation rates are so extreme, $\geq 10^3 M_{\odot} \text{ year}^{-1}$, that a significant fraction of the stars in the QSO host galaxy can be formed in $< 10^9$ years.

Alternatively, the dust may be heated by radiation from the AGN. Sanders et al. (1989) argue that radiation from the AGN is the dominant dust heating mechanism, since in most cases it requires the absorption of only a small fraction ($\leq 20\%$) of the AGN UV

luminosity by dust, even for the high redshift sources (Carilli et al. 2000). An important constraint on AGN dust heating models is provided by the minimum size of about 1 kpc for the dust emission region one derives from the observed luminosity and dust temperature (see section 3). Hence, while the optical ‘big blue bump’ emission is thought to arise in a hot ($10^{4.5}$ K) accretion disk on pc-scales, the rest-frame far IR emission must be due to warm dust on kpc-scales. In the Sanders et al. (1989) model for AGN-powered IR emission from QSOs, dust heating on kpc scales is accomplished by assuming that the dust is distributed in a kpc-scale warped disk, thereby allowing UV radiation from the AGN to illuminate the outer regions of the disk. An alternate mechanism for large-scale dust heating has been proposed by Maloney, Hollenbach, & Tielens (1996) in which hard X-rays penetrate the very high column density gas in the vicinity of the AGN.

In this paper we present extensive observations at cm and mm wavelengths of a sample of high redshift QSOs from the Sloan Digital Sky Survey (SDSS; York et al. 2000). Our observations include sensitive radio continuum imaging at 1.4 and 43 GHz with the Very Large Array (VLA), and photometry at 250 GHz using the Max-Planck Millimeter Bolometer array (MAMBO) at the IRAM 30m telescope. These observations are a factor three more sensitive than previous studies of high redshift QSOs at these frequencies (Schmidt et al. 1995b; Omont et al. 1996a; Stern et al. 2000). Details of the multifrequency radio continuum imaging will be given elsewhere (Rupen et al. 2001, in preparation). In this paper we present the radio results that are relevant to the analysis and interpretation of the dust continuum emission. We compare the dust emission properties of these sources with their optical and radio continuum and spectral properties, and with those of lower redshift sources. We assume $H_0 = 50 \text{ km s}^{-1} \text{ Mpc}^{-1}$, $q_0 = 0.5$, $\Lambda = 0$, and we define the spectral index, α , as a function of frequency, ν , as: $S_\nu \propto \nu^\alpha$.

2. The Sample

The QSO sample is the result of optical spectroscopy of objects of unusual color from the northern Galactic Cap and the Southern Equatorial Stripe of the SDSS. The survey has yielded over 100 QSOs with $z \geq 3.6$, including eight of the ten highest redshift QSOs known (Fan et al. 1999, 2000b, 2001a,b; Schneider et al. 2000a,b, 2001; Zheng et al. 2000).

We observed 41 of these high redshift QSOs, taken from Fan et al. (1999), Fan et al. (2000a), and Schneider et al. (2000a). The QSO properties are listed in Table 1. The observed sources span a range of $M_B = -26.1$ to -28.8 , and a redshift range of $z = 3.6$ to 5.0. Comparative numbers for the APM sample of 16 QSOs observed by Omont et al. (1996a) are $M_B = -26.8$ to -28.5 , and $z = 4.0$ to 4.7.

The sources in Table 1 have a mean optical spectral power law index, $\alpha = -0.67$, with a dispersion of 0.29, a mean redshift, $z = 4.20$, with a dispersion of 0.44, and a mean absolute blue magnitude, $M_B = -27.07$, with a dispersion of 0.57. We can compare these values to those of the 39 QSOs at $z > 3.6$ from the SDSS Fall Equatorial stripe presented in Fan et al. (2001b). The Fall Equatorial stripe sample is a statistically complete sample of high- z QSOs selected according to the same criteria as the sources listed in Table 1. The Fall Equatorial stripe sample has a mean optical spectral power law index, $\alpha = -0.79$, with a dispersion of 0.34, a mean redshift, $z = 4.06$, with a dispersion of 0.39, and a mean absolute blue magnitude, $M_B = -26.82$, with a dispersion of 0.58. Hence, within the scatter of the distributions, the sources in Table 1 can be considered representative of the complete high- z QSO sample from the Fall Equatorial stripe.

3. Observations

Observations were made using MAMBO (Kreysa et al. 1999) at the IRAM 30m telescope on Pico Veleta in Spain, in December 1999 and February 2000. MAMBO is a 37 element bolometer array sensitive between 190 and 315 GHz. The half-power sensitivity range is 210 to 290 GHz, but the overall profile is asymmetric, with a sharp rise in sensitivity at low frequency, then a gradual decrease in sensitivity to higher frequency. Convolving the frequency response of the bolometer array with the atmospheric transmission curve (which also decreases with increasing frequency), and with the rising spectrum of a typical dust emitting source at high redshift, leads to an effective central frequency of 250 GHz. The beam for the feed horn of each bolometer is matched to the telescope beam of $10.6''$, and the bolometers are arranged in a hexagonal pattern with a beam separation of $22''$. Observations were made in standard on-off mode, with 2 Hz chopping of the secondary by $50''$ in azimuth. The data were reduced using the MOPSI software package of the Max-Planck-Institut für Radioastronomie (Zylka 1998). Pointing was monitored every hour, and was found to be repeatable to within $2''$. The sky opacity was monitored every hour; zenith optical depths ranged between 0.23 and 0.36. Gain calibration was performed using observations of Mars, Uranus, and Ceres. We estimate a 20% uncertainty in absolute flux density calibration based on these observations. The target sources were centered on the central bolometer in the array, and the temporally correlated variations of the sky signal (sky noise) detected in the remaining bolometers were subtracted from all the bolometer signals. The total on-target plus off-target observing times for the sources are listed in Table 1. The typical rms sensitivity in 1 hour was 0.5 mJy for the on-source bolometer beam.

The 1.4 GHz VLA observations were made in the A (30 km) and BnA (mixed 30 km and 10 km) configurations on July 8, August 14, September 30, and October 8, 1999,

using a total bandwidth of 100 MHz with two orthogonal polarizations. Each source was observed for a total of 2 hours, with short scans made over a large range in hour angle to improve Fourier spacing coverage. Standard phase and amplitude calibration were applied, as well as self-calibration using background sources in the telescope beam. The absolute flux density scale was set using observations of 3C 48. The final images were generated using the wide field imaging and deconvolution capabilities of the AIPS task IMAGR. The theoretical rms noise value is between 20 and $30 \mu\text{Jy beam}^{-1}$, depending on the range of telescope elevations over which the source was observed, and for about half the sources the measured noise values are in this range. For the remaining sources, the noise levels are significantly higher due to side-lobe confusion by bright sources. The Gaussian restoring CLEAN beams were between $1.5''$ and $3''$ FWHM.

Some of the sources had previous VLA detections as part of the FIRST survey (SDSS J1053-0016, SDSS J1235-0003, SDSS J1412-0101; Becker, White, & Helfand 1995). We re-observed these sources, and obtained the same flux densities to within 15% of the FIRST values in all cases.

We chose four of the dust emitting sources, (SDSS J0150+0041, SDSS J0255+0048, SDSS J0338+0021, SDSS J1112+0050) as a sub-sample for 43 GHz observations, in order to search for high frequency, flat spectrum emission that might be synchrotron self-absorbed at 1.4 GHz. Observations were made on Feb 20, 2000, using the VLA in the B (10 km) configuration in standard continuum mode. Fast switching phase calibration was employed (Carilli & Holdaway 1999), and observing times were 0.5 hr at 43 GHz, resulting in an rms noise of $0.35 \text{ mJy beam}^{-1}$.

4. Results and Analysis

The results of our 250 GHz survey of high redshift QSOs are given in Table 1. These include: (i) flux densities at 250 GHz (S_{250} ; column 3), (ii) flux densities at 1450 Å (S_{1450} ; column 4), (iii) flux densities at 1.4 GHz at the position of the optical QSO ($S_{1.4}$; column 5), (iv) absolute blue magnitudes (column 6; Fan et al. 1999, 2000a), (v) observing time at 250 GHz, and (vi) notes on source properties (column 8). In the following analysis we consider a source with a measured flux density three times greater than the rms noise (3σ) to be a valid detection. Such sources are marked with an asterisk in Table 1. We should also point out that the mm, cm, and optical observations were not simultaneous, and hence that variability could affect the observed spectra at some level.

We detect 16 of the 41 sources at $S_{250} \geq 1.4$ mJy. Only four of the sources have $S_{250} \geq 3$ mJy. A higher detection rate at the limit of $S_{250} \geq 3$ mJy was found in the survey of the APM QSO sample by Omont et al. (1996), in which they detected 6 of 16 sources. This difference in detection rates appears to be statistically significant: if there were a true universal fraction of 10% of high- z QSOs with $S_{250} \geq 3$ mJy, then there is about a 1% chance that in 16 objects 6 or more would meet this criterion. The optical/near IR color selection criteria for the APM sample are similar to those of the SDSS sample. The one significant difference is that the rest frame blue luminosities for the APM are somewhat higher on average (by about 0.5 mag), than those of the SDSS sources in Table 1 (see section 2). However, given the lack of a strong correlation between M_B and S_{250} (see Figure 2 below), the cause for the possibly higher detection rate at high S_{250} for the APM sample relative to the SDSS sample remains unknown. Further observations of the mm properties of high z QSOs that are in progress may clarify this issue (Omont et al. 2001).

Considering the radio properties of the sources in Table 1, nine sources in Table 1 are detected at 1.4 GHz at $\geq 3\sigma$. For the nine radio-detected sources in Table 1, eight

are unresolved, with size limits (FWHM) of about 1'', while SDSS J0232-0000 is possibly extended, with a size $\sim 1.3''$. Miller et al. (1990) suggested a division between radio loud and radio quiet QSOs at a rest frame 5 GHz spectral luminosity of 10^{33} erg s $^{-1}$ Hz $^{-1}$. This corresponds to a flux density of $S_{1.4} = 1$ mJy for a source at $z = 4.2$ assuming a radio spectral index of -0.8 . According to this criterion, 2 of 16 SDSS QSOs detected at 250 GHz can be considered radio-loud (SDSS J1235-0003 and SDSS J1412-0101), while 2 of 25 sources not detected at 250 GHz can be considered radio-loud (SDSS J0153-0011 and SDSS J1053-0016). Both fractions are consistent with the value of 10% of optically selected high redshift QSOs being radio loud according to this criterion (Schmidt et al. 1995b; Stern et al. 2000).

4.1. Evidence for thermal dust emission at 250 GHz

We first address the question of whether the 250 GHz emission is thermal dust emission, or non-thermal synchrotron radiation. For most of the sources detected at 250 GHz, the 1.4 GHz flux density (or upper limit) is an order of magnitude or more below the 250 GHz flux density. Two of the sources have 1.4 GHz flux densities comparable to, or larger than, the 250 GHz flux density. The source SDSS J1412-0101 has $S_{1.4} = 3.9$ mJy and $S_{250} = 4.5$ mJy. Observations of this source at 8.4 GHz revealed a 1.1 mJy source (Rupen et al. 2001), such that the cm source has a falling spectrum of index -0.7 , making it unlikely that the mm continuum is a continuation of the synchrotron emission spectrum from the AGN. The source SDSS J1235-0003 has $S_{250} = 1.6$ mJy, and $S_{1.4} = 4.5$ mJy. Observations on the same day as those at 1.4 GHz found a 5 GHz flux density of $S_5 = 17$ mJy, and a 15 GHz flux density of $S_{15} = 7$ mJy. The source was unresolved at all frequencies. In this case, it remains possible that the 250 GHz emission is non-thermal.

It is possible that emission from a compact AGN could be synchrotron self-absorbed

at low frequency. To check this idea, we performed 43 GHz observations of 4 of the 250 GHz detected sources, as listed in section 3; none of the sources were detected. Assuming a 2σ upper limit of 0.7 mJy at 43 GHz implies a rising spectrum between 43 and 250 GHz of index $\alpha > 0.5$. While this limit is well below the index expected for thermal dust emission ($\alpha_{43}^{250} \approx 3$ for a source at $z = 4.2$), it does argue against compact, synchrotron self-absorbed sources as the origin of the 250 GHz emission, as such sources typically show mm spectral indices $\alpha_{\text{mm}} \sim 0 \pm 0.3$ (Sanders et al. 1989). In the following discussion we will assume that the 250 GHz emission from the sources in Table 1 is thermal dust emission, with the possible exception of SDSS J1235–0003. These data imply that in mm surveys of high redshift QSOs, the fraction of flat spectrum, radio loud AGN with synchrotron emission extending into the mm-regime is at most a few percent. Studies of lower redshift QSOs show that the fraction of flat spectrum radio loud sources in optically selected samples is also only a few percent (Hopkins et al. 1999).

A source with $S_{250} = 1$ mJy at $z = 4.2$ and a dust spectrum of the type seen in the low redshift starburst galaxy Arp 220 (corresponding roughly to a modified black body spectrum of dust emissivity index = 1 and temperature = 50 K) has an FIR luminosity, L_{FIR} , of $1.1 \times 10^{12} L_{\odot}$, where L_{FIR} corresponds to the integrated luminosity between 42 and 122 μm (Condon 1992). If we assume that star-formation is the mechanism giving rise to the dust emission, we can use the relations in Omont et al. (2001) and Carilli et al. (2001) to derive the dust mass, M_{D} , and total star formation rate, SFR, from S_{250} . The relations are: $M_{\text{D}} = 1.1 \times 10^8 \times S_{250} M_{\odot}$, and $\text{SFR} = 360 \times S_{250} M_{\odot} \text{ year}^{-1}$, with S_{250} in mJy. This again assumes $T_{\text{D}} = 50$ K.

A conservative lower limit to the solid angle, Ω_s , of a dust emitting source can be derived from the observed flux density making the extreme assumption of optically thick emission (Downes et al. 1999). Assuming $T_{\text{D}} \sim 50$ K (Benford et al. 1999) and $z \sim 4$, leads

to: $\Omega_s > 0.0043 S_{250} \text{ arcsec}^2$, where S_{250} is the 250 GHz flux density in mJy. This implies absolute lower limits to the angular diameters of the sources in Table 1 between $0.08''$ and $0.15''$, corresponding to physical sizes of 0.5 to 1 kpc. Given the likelihood that the observed 250 GHz emission is from an optically thin grey body, it is almost certain that the sources are larger than these lower limits. Also, this size corresponds to the total emitting area. Multiple smaller regions within the $10.6''$ telescope beam are certainly possible (see section 5). Observations at mm wavelengths with sub-arcsecond resolution are required to constrain the source sizes.

4.2. Trends with Redshift and M_B

Figure 1 shows values of S_{250} versus redshift for the 41 QSOs in Table 1. The solid line is the expected flux density of Arp 220. This curve shows clearly the effect of the large ‘inverse K ’ correction for thermal dust emission at mm and submm wavelengths, with the observed flux density of a source such as Arp 220 remaining roughly constant over the observed redshift range (Blain and Longair 1993). There is an interesting trend for a lower detection rate for the SDSS QSOs with increasing redshift: for $z < 4.4$ we detect 14 of 28 sources while for $z > 4.4$ we detect 2 of 13 sources. A larger sample of sources, over a larger redshift range, is required to verify this trend.

Figure 2 shows values of L_{FIR} versus M_B for the 41 QSOs in Table 1. At the limit of $L_{\text{FIR}} > 1.8 \times 10^{12} L_\odot$, we detect 9 of 23 sources with $M_B > -27$, and 7 of 17 sources with $M_B < -27$. This is consistent with the lack of a strong correlation between M_B and L_{FIR} in the lower redshift, lower optical luminosity sample of Palomar-Green (PG) QSOs presented by Sanders et al. (1989; see also Chini, Kreysa, & Biermann 1989), and is indicative of the large scatter in the dust properties of QSOs in general (see Figure 4 below), and the relatively narrow range in M_B in Figure 2.

4.3. Comparison to the Radio-to-FIR Correlation for Star Forming Galaxies

Figure 3 shows the relationship between redshift and the 250-to-1.4 GHz spectral index for a star forming galaxy taken from the model of Carilli & Yun (2000) based on 17 low redshift galaxies (roughly equivalent to a modified black body spectrum with $T_D = 50\text{K}$ and dust emissivity index = 1.5). The relationship relies on the tight radio-to-FIR correlation seen for star forming galaxies in the nearby universe (Condon 1992). The dotted curve gives the rms scatter for the 17 galaxies. The solid symbols are the results for the SDSS QSOs detected at 250 GHz, while the open symbols are for the APM QSO sample from Omont et al. (1996) and Yun et al. (2000). The arrows indicate non-detections in the radio, and hence lower limits to the spectral index. On this diagram, a point located below the curve would indicate a source that is radio-loud relative to the standard radio-to-FIR correlation for star forming galaxies, while a point located above the curve would indicate a source which is radio-quiet relative to this relationship (Condon 1992). The lower limits are below the curve, and hence are consistent with a star forming galaxy spectrum, although a factor two better sensitivity at 1.4 GHz is required to provide more stringent constraints in this regard.

The radio-detected QSOs fall below the star forming galaxy curve in Figure 3. Two of the sources (SDSS J1235–0003 and SDSS J1412–0101) are clearly radio loud AGN (see section 4.0). The fainter radio detections may indicate radio emission from the AGN, but at a level below that required for the source to be defined as radio loud according to Miller et al. (1990). An alternative explanation for these sources is a warmer dust component: increasing the dust temperature by a factor two or so could give rise to the observed offset with respect to the model in Figure 3 (Blain 1999).

4.4. Spectral Energy Distributions

Figure 4 shows the mean radio-through-optical Spectral Energy Distributions (SEDs) for radio-loud and radio-quiet QSOs derived from observations of a large sample of PG QSOs by Sanders et al. (1989). The solid curve shows the SED for radio loud QSOs, while the dashed curve shows the SED for radio quiet QSOs. The hatched regions indicate the scatter in the measured values for the PG sample. Note that the QSOs in the PG sample are typically an order of magnitude less luminous in the rest-frame UV than the high redshift sources, with most of the PG sources in the range: $M_B = -23$ to -27 .

The data points in Figure 4 show the results for the mm detections in the SDSS and APM QSO samples, normalized by their blue spectral luminosities. The normalized mm detections all fall within the range defined by the PG sample. The upper limits for the non-detected sources at 250 GHz would fall at the low end of the range defined by the Sanders et al. (1989) SEDs.

The two radio loud SDSS QSOs according to the Miller et al. (1990) definition detected at 250 GHz are clearly evident in the normalized SEDs in Figure 4, while the normalized upper limits for the non-detected sources at 1.4 GHz are consistent with the Sanders et al. (1989) radio quiet QSO SED. The remaining three radio-detected SDSS QSOs in Figure 4 fall in-between the radio quiet and radio loud SEDs, as do the QSOs from the APM sample. The large gap between the radio loud and radio quiet SEDs from Sanders et al. (1989), as reproduced in Figure 4, represents the possible bi-modality of the radio properties of QSOs, as suggested by Stocke et al. (1992). The reality of this bi-modality has been called into question recently by White et al. (2000), and Stocke et al. (1992) show that the bi-modality is less clearly delineated for high blue luminosity QSOs relative to lower luminosity sources. Further analysis of the radio detections within this sample, including studies of radio spectra and spatial structure, will be given in Rupen et al. (2001).

4.5. Broad Absorption Lines

Omont et al. (1996a) suggest a possible correlation between the Broad Absorption Line (BAL) phenomenon and thermal dust emission in QSOs. In the APM sample of Omont et al. (1996a), two of six sources detected at 250 GHz have BAL features. The BAL fraction for high z QSOs in general is about 10% (Fan et al. 2001a).

Our data on the SDSS sample provide only marginal support for this idea, with 4 of the 16 sources detected at S_{250} GHz showing evidence for BAL features, as compared to 3 sources with BALs out of the 25 non-detected sources at 250 GHz.

5. Discussion

We detect 16 of 41 high redshift QSOs from the SDSS survey with $S_{250} \geq 1.4$ mJy. Assuming $T_D = 50$ K, we show that the 250 GHz emission is most likely thermal emission from warm dust on a scale > 1 kpc in the host galaxy of the QSO. The implied dust masses for the sources are in the range of 1.5 to $5.9 \times 10^8 M_\odot$. If the dust is heated by star formation, the star formation rates are in the range 500 to $2000 M_\odot$ year $^{-1}$. Sensitive radio observations show a radio-loud fraction (according to the definition of Miller et al. 1990) for the sample as a whole of 10%, consistent with previous observations of high redshift QSOs, with no clear relationship between dust emission and radio-loud QSOs.

The blue-normalized optical-through-radio SEDs for these sources are within the broad range delineated by the PG sample of lower redshift, lower luminosity QSOs (Figure 4). This result suggests that for the sources detected at 250 GHz, we are not seeing a major new broad-band spectral emission ‘feature’ in high redshift QSOs relative to the SEDs of lower redshift QSOs. Conversely, the blue-normalized limits for the non-detections at 250 GHz in the SDSS high z QSO sample are at the low end of the distribution defined

by low z QSOs, leaving open the possibility of a population of high z sources which are under-luminous in the rest frame submm relative to the SED of low z QSOs. While this result could be used to argue against models involving a major burst of star formation in the host galaxies of high redshift QSOs, the large scatter in the mm SEDs could effectively mask such a phenomenon. Also, Sanders et al. (1989) point out that from cm to submm wavelengths, the radio quiet SED model based on the PG QSO sample is consistent with the observed SEDs for star forming galaxies.

A number of studies have addressed the question of the dust heating mechanism in high z AGN by SED modeling, with mixed results. Radiative transfer models by Rowan-Robinson (1999) suggest that the observed SEDs at rest frame wavelengths $> 50\mu\text{m}$ are consistent with an extreme starburst model for most high redshift dust emitting QSOs. On the other hand, models by Andreani et al. (1999) and Willott et al. (1999) suggest that the dust emission spectra from $3\mu\text{m}$ to $30\mu\text{m}$ can be explained by dust heated by the AGN. The cm-to-mm SEDs may also indicate star formation in a few sources (Yun et al. 2000), however the radio limits in most sources are inadequate to constrain such a model (Figure 3). Mid-infrared spectroscopy using the Space Infrared Telescope Facility of the PAH features and other spectral lines may provide a star formation vs. AGN diagnostic (Genzel et al. 1998).

Spatially resolved observations may be critical in addressing this issue, since a dust emitting region spatially distinct from the optical QSO can be used to argue for at least some dust heating by star formation. Such an argument has been used convincingly in the case of CO and dust emission in the vicinity of a number of high redshift radio galaxies and AGN (Papadopoulos et al. 2000, 2001; Ivison et al. 2000). To date, the only high redshift QSO in which such a spatial segregation has been observed is the $z = 4.7$ QSO BR1202-0725, in which the cm and mm continuum, and the CO line emission, show two

sources of roughly equal strength separated by 4'', while the optical line and continuum emission is restricted to a single source (Hu, McMahon, & Egami 1996; Omont et al. 1996b; Ohta et al. 1996; Yun et al. 2000; Kohno et al. 2000, in preparation).

The question of the dominant dust heating mechanism, ie. AGN versus star formation, is difficult to answer for low redshift sources (Rigopoulou et al. 1999). Addressing the question at high redshift is just that much more difficult. The sources detected at 250 GHz in Table 1 present an ideal opportunity for addressing this issue in detail. A number of follow-up observations of these sources are required to properly address this question, including: (i) more sensitive radio continuum observations to better characterize the cm-to-mm SEDs, (ii) submm observations to determine the dust temperature, (iii) high resolution (sub)mm observations to determine the spatial distribution of the dust, and (iv) CO observations to better constrain the gas mass and kinematics. Such observations are at the limit of what is possible with current instrumentation, but will become routine with the expanded VLA and the Atacama Large Millimeter Array.

The VLA is a facility of the National Radio Astronomy Observatory (NRAO), which is operated by Associated Universities, Inc. under a cooperative agreement with the National Science Foundation. This work was based on observations carried out with the IRAM 30 m telescope. IRAM is supported by INSU/CNRS (France), MPG (Germany) and IGN (Spain). This research made use of the NASA/IPAC Extragalactic Data Base (NED) which is operated by the Jet Propulsion Lab, Caltech, under contract with NASA. CC acknowledges support from the Alexander von Humboldt Society. DPS acknowledges support from National Science Foundation Grant AST99-00703. XF and MAS acknowledge support from the Research Corporation, NSF grants AST96-16901 and AST00-71091 and an Advisory Council Scholarship.

REFERENCES

Andreani, P., Franceschini, A., & Granato, G. 1999, MNRAS, 306, 161

Begelman, M., Blandford, R., & Rees, M. 1984, Rev. Mod. Phys., 56, 255

Becker, R.H.. White, R.L., & Helfand, D.J. 1995, ApJ, 450, 559

Benford, D. J., Cox, P., Omont, A., Phillips, T. G., & McMahon, R. G. 1999, ApJ (letters), 518, 65

Blain, A.W., & Longair, M.S. 1993, MNRAS, 264, 509

Blain, A.W. 1999, MNRAS, 309, 955

Blain, A.W., Jameson, A., Smail, I., Longair, M.S., Kneib, J.-P., & Ivison, R.J. 1999, MNRAS, 309, 715

Boyle, B.J. & Terlevich, R.J. 9198, MNRAS, 293, 49

Carilli, C.L., Miller, N., Poggianti, B., and Owen, F. 2001, in preparation

Carilli, C.L. et al. 2000, ApJ (letters), 533, 13

Carilli, C. L. & Yun, M. S. 2000, ApJ, 530, 618 (erratum: 539, 1024)

Carilli, C.L. & Holdaway, M.A. 1999, Radio Science, 34, 817

Carilli, C. L., Menten, K.M. & Yun, M. S. 1999, ApJ (letters), 521, 25

Carilli, C.L., Wrobel, J., & Ulvestad, J. 1999, AJ, 115, 928

Carilli, C. L. & Yun, M. S. 1999, ApJ (letters), 513, 13

Chini, R., Kreysa, E., & Biermann, P.L. 1989, A&A, 219, 87

Condon, J.J. 1992, ARAA, 30, 575

Downes, D. et al. 1999, A&A, 347, 809

Dunlop, D. 2000, in *Deep mm Surveys*, eds. J. Lowenthal & D. Hughes (World Scientific), in press

Fan, X. et al. 1999, AJ, 118, 1

Fan, X. et al. 2000, AJ, 119, 1

Fan, X. et al. 2001a, AJ, 121, 31

Fan, X. et al. 2001b, AJ, 121, 54

Ferrarese, L. & Merritt, D. 2000, ApJ (letters), 539, 9

Franceschini, A., Hasinger, G., Mayaji, T., & Malquori, D. 1999, MNRAS (letters), 310, 5

Gebhardt, Karl et al. 2000, ApJ (letters), 539, 13

Genzel, R. et al. 1998, ApJ, 498, 579

Ghez, A.M., Klein, B.L., Mooris, M., & Becklin, E.E. 1998, ApJ, 509, 678

Genzel, R., Pichon, C., Eckart, A., Gerhard, P. & Ott, T. 2000, MNRAS, 317, 348

Granato, G.L. et al. 2000, MNRAS, in press

Greenhill, L.J., Gwinn, D.R., Antonucci, R., & Barvainis, R. 1996, ApJ (letters), 472, 21

Guilloteau, S., Omont,A., McMahon, R.G., Cox,P., & Petitjean,P. 1997, A&A, 328, L1

Guilloteau, S., Omont,A., McMahon, R.G., Cox,P., & Petitjean,P. 1999, A&A, 349, 363

Helfand, D.J., Becker, R.H., Gregg, M.D., Laurent-Muehleisen, S., Brotherton, M., & White, R.L. 1999, BAAS, 195, 1701

Helfand, D.J. et al. 1997, BAAS, 190, 4304

Hooper, E.J., Impey, C.D., Foltz, C.B., & Hewett, P.C. 1995, ApJ, 445, 62

Hopkins, A., Mobasher, B., Cram, L., & Rowan-Robinso, M. 1998, MNRAS, 296, 839

Hu, E.M., McMahon, R.G., & Egami, E. 1996, ApJ (letters), 459, 53

Ivison, R.J., Dunlop, J.S., Smail, I., Dey, A., Lui, M.C., Graham, J. 2000, *ApJ*, in press
(*astroph* 0005234)

Kellermann, K.I., Sramek, R., Schmidt, M., Shaffer, D.B., & Green, R. 1989, *AJ*, 98, 1195

Kennefick, J.D., Djorgovski, S.G., and de Carvalho, R.R. 1995, 110, 2553

Kormendy, John 2000, *Science*, in press

Kormendy, John, & Ho, Luis C. 2000, in *The Encyclopedia of Astronomy and Astrophysics*
(Institute of Physics Publishing), in press

Kreysa, E. et al. 1999, *SPIE*, 3357, 319

Magorrian, J. et al. 1998, *AJ*, 115, 2285

Maloney, P.R., Hollenbach, D.J., & Tielens, A.G. 1996, *ApJ*, 466, 561

Miller, L., Peacock, J.A., & Mead, A.R. 1990, *MNRAS*, 244, 207

Miyoshi, M., et al. 1995, *Nature*, 373, 127

Ohta, K., Yamada, T., Nakanishi, K., Kohno, K., Akiyama, M., & Kawabe, R. 1996,
Nature, 382, 426

Omont, A., McMahon, R. G., Cox, P., Kreysa, E., Bergeron, J., Pajot, F., & Storrie-
Lombardi, L.J. 1996a, *A&A*, 315, 1

Omont, A., Petitjean, P., Guilloteau, S., McMahon, R. G., Solomon, P. M., & Pecontal, E.
1996b, *Nature*, 382, 428

Omont, A. et al. 2001, *A&A*, submitted

Papadopoulos, P.P. et al. 2000, *ApJ*, 528, 626

Papadopoulos, P.P., Ivison, R.J., Carilli, C.L., & Lewis, G. 2001, *Nature*, 409, 58

Richstone, D. et al. 1998, *Nat. Supp.*, 395A, 14

Rigopoulou, D., Spoon, H.W., Genzel, R., Lutz, D., Moorwood, A., & Tran, Q.D. 1999, AJ, 118, 2625

Rowan-Robinson, M. 2000, MNRAS, 316, 885

Rowan-Robinson, M. et al. 1997, MNRAS, 298, 490

Rocca-Volmerange, B., Guiderdoni, B., Dennefeld, M., & Van, Tran-Thanh 1993, *First Light in the Universe*, (Editions Frontieres, Cedex, France)

Sanders, D.B. & Mirabel, I.F. 1996, ARAA, 34, 749

Sanders, D.B., Phinney, E.S., Neugebauer, G., Soifer, B.T., & Matthews, K. 1989, ApJ, 347, 29

Schmidt, M., Schneider, D.P., & Gunn, J.E. 1995a, AJ, 110, 68

Schmidt, M., van Gorkom, J.H., Schneider, D.P., & Gunn, J.E. 1995b, AJ, 109, 473

Schneider, D.P. et al. 2000a, PASP, 112, 6

Schneider, D.P. et al. 2000b, AJ, 120, 2183

Schneider, D.P. et al. 2001, AJ, in press

Songaila, A., Hu, E.M., Cowie, L.L., & McMahon, R.G. 1999, ApJ (letters), 525, 5

Stern, D., Djorgovski, S.G., Perley, R.A., de Carvalho, R.R., & Wall, J.V. 2000, AJ, 119, 1526

Stocke, J.T., Morris, S.L., Weymann, R.J., & Foltz, C.B. 1992, ApJ, 396, 487

Tanaka, Y. et al. 1995, Nature, 375, 659

White, R.L. et al. 2000, ApJ (supplement), 126, 133

Willott, C.J., Rawlings, S., & Jarvis, M.J. 2000, 313, 237

York, D.G. et al. 2000, AJ, 120, 1588

Yun, M.S., Carilli, C.L., Kawabe, R., Tutui, Y., Kohno, K. & Ohta, K. 2000, ApJ, 528, 171

Zylka, R. 1998, *MOPSI Users Manual*, (IRAM: Grenoble)

Table 1: SDSS High Redshift QSOs

Source	z	$S_{250 \text{ GHz}}$	$S_{1450 \text{ \AA}}$	$S_{1.4 \text{ GHz}}$	M_B	Obs. time	Notes
SDSS		mJy	mJy	mJy		sec	
J003525.29+004002.8	4.75	0.3 ± 0.5	0.038	0.024 ± 0.027	-26.66	3500	
J010619.25+004823.4	4.43	-0.4 ± 0.4	0.121	$0.601 \pm 0.043^{*,a}$	-27.70	4640	DPOSS/APM
J012403.78+004432.7	3.81	$2.0 \pm 0.3^*$	0.215	0.11 ± 0.048	-28.19	5740	
J012650.77+011611.8	3.66	-0.6 ± 0.6	0.056	$0.21 \pm 0.023^*$	-26.62	2180	
J015048.83+004126.2	3.67	$2.2 \pm 0.4^*$	0.160	-0.004 ± 0.019	-27.75	4590	BAL
J015339.61-001104.9	4.20	0.9 ± 0.5	0.100	$5.3 \pm 0.041^*$	-27.27	3210	
J021102.72-000910.3	4.90	0.5 ± 0.3	0.039	0.033 ± 0.030	-26.63	7650	
J023231.40-000010.7	3.81	$1.8 \pm 0.3^*$	0.043	$0.066 \pm 0.022^*$	-26.54	7350	
J025112.44-005208.2	3.78	$2.4 \pm 0.6^*$	0.058	-0.03 ± 0.024	-26.74	2170	
J025518.58+004847.6	3.97	$2.1 \pm 0.4^*$	0.125	0.043 ± 0.031	-27.67	3350	BAL
J031036.97-001457.0	4.63	-0.5 ± 0.4	0.035	0.068 ± 0.025	-26.78	4490	
J032608.12-003340.2	4.16	$1.5 \pm 0.4^*$	0.080	0.068 ± 0.025	-27.21	4770	DPOSS/APM
J033829.31+002156.3	5.00	$3.7 \pm 0.3^*$	0.047	0.037 ± 0.025	-26.56	8000	BAL ^b
J105320.43-001649.3	4.29	0.1 ± 0.2	0.063	$11.5 \pm 1.0^*$	-27.04	10360	DPOSS/APM
J111246.30+004957.5	3.92	$2.7 \pm 0.5^*$	0.091	$0.364 \pm 0.050^*$	-27.50	2830	
J111401.48-005321.1	4.58	0.2 ± 0.3	0.047	-0.036 ± 0.028	-26.82	6880	
J112253.51+005329.8	4.57	-0.1 ± 0.3	0.076	0.096 ± 0.040	-27.35	10030	
J120441.73-002149.6	5.03	0.6 ± 0.4	0.087	0.064 ± 0.046	-27.64	4300	
J122600.68+005923.6	4.25	$1.4 \pm 0.4^*$	0.086	0.016 ± 0.027	-27.36	4850	
J123503.04-000331.8	4.69	$1.6 \pm 0.4^*$	0.028	$18.8 \pm 0.4^*$	-26.29	6320	

^aAn astrisk indicates a 3σ detection. ^bSongaila et al. 1999

Source	z	$S_{250 \text{ GHz}}$	$S_{1450 \text{ \AA}}$	$S_{1.4 \text{ GHz}}$	M_B	Obs. time	Notes
SDSS		mJy	mJy	mJy		sec	
J131052.52–005533.4	4.14	-0.3 ± 0.5	0.097	-0.11 ± 0.22	–27.46	2380	
J132110.82+003821.7	4.70	0.4 ± 0.4	0.033	0.036 ± 0.030	–26.47	4425	
J140554.07–000037.0	3.55	1.0 ± 0.4	0.120	0.005 ± 0.047	–27.40	4540	BAL
J141205.78–010152.6	3.73	$4.5 \pm 0.7^*$	0.068	$3.9 \pm 0.2^*$	–26.91	2160	BAL
J141315.36+000032.1	4.08	2.0 ± 0.8	0.034	0.040 ± 0.030	–26.30	1664	
J141332.35–004909.7	4.14	$2.5 \pm 0.5^*$	0.070	0.009 ± 0.027	–27.10	3730	BAL
J142329.98+004138.4	3.76	0.4 ± 0.8	0.046	0.003 ± 0.028	–26.49	1270	
J142647.82+002740.4	3.69	$3.9 \pm 0.8^*$	0.056	0.055 ± 0.033	–26.69	1290	
J144428.67–012344.1	4.16	-0.4 ± 0.7	0.052	-0.003 ± 0.027	–26.80	2060	
J144758.46–005055.4	3.80	$5.4 \pm 0.8^*$	0.051	0.050 ± 0.024	–26.62	1160	
J151618.44–000544.3	3.70	-0.1 ± 0.6	0.033	0.050 ± 0.045	–26.11	3220	
J152740.52–010602.6	4.41	-0.1 ± 0.5	0.052	0.005 ± 0.025	–26.87	3690	
J153259.96–003944.1	4.62	0.2 ± 0.7	0.063	$< 0.06^c$	–27.16	1418	
J160501.21–011220.0	4.92	0.1 ± 0.4	0.061	$< 0.06^c$	–27.23	4590	BAL
J161926.87–011825.2	3.84	$2.3 \pm 0.6^*$	0.047	0.047 ± 0.025	–26.54	2560	
J162116.91–004251.1	3.70	0.1 ± 0.3	0.394	0.019 ± 0.027	–28.81	5990	
J165527.61–000619.2	3.99	-0.1 ± 0.4	0.036	0.010 ± 0.033	–26.33	3414	
J225419.23–000155.0	3.68	0.3 ± 0.4	0.063	-0.010 ± 0.050	–26.73	5650	
J225759.67+001645.7	3.75	0.4 ± 0.4	0.086	-0.022 ± 0.10	–27.19	5520	
J230952.29–003138.9	3.95	-0.2 ± 0.5	0.058	0.088 ± 0.044	–26.82	3925	
J235718.35+004350.4	4.34	$1.8 \pm 0.6^*$	0.041	$0.110 \pm 0.027^*$	–26.59	2650	

^c3 σ limits at 5 GHz (see Fan et al. 1999 for a detailed discussion of J1532–0039).

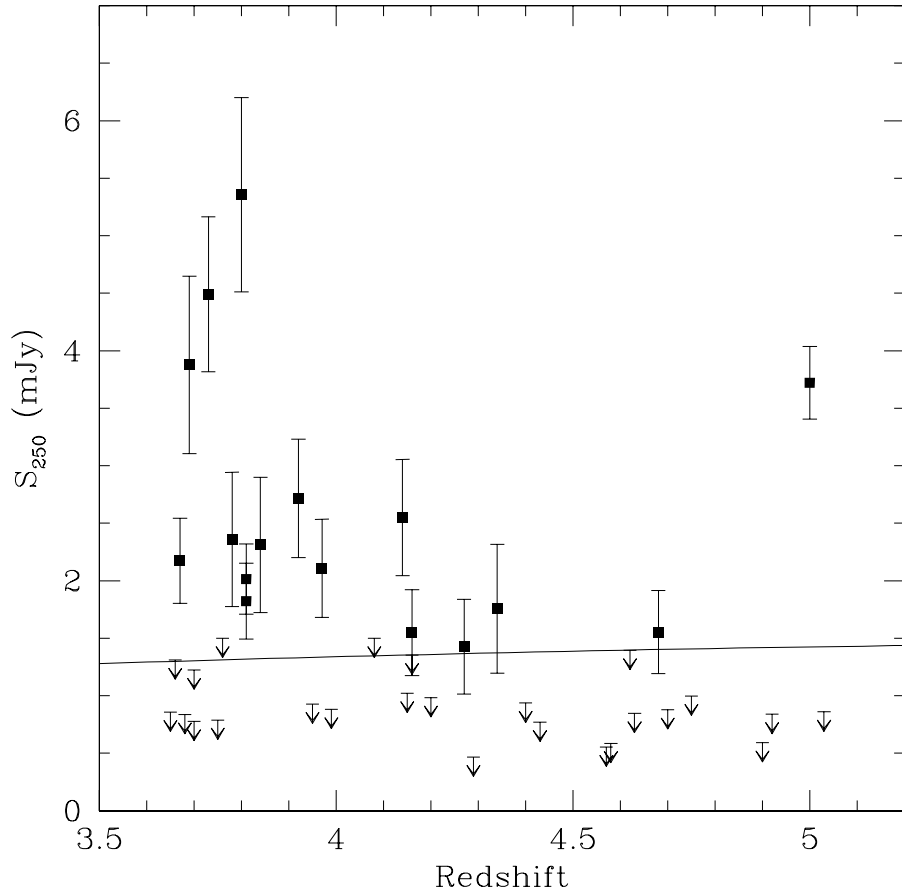


Fig. 1.— The relationship between redshift and S_{250} for the SDSS high redshift QSOs listed in Table 1. The squares with error bars indicate sources detected at $> 2\sigma$. The arrows represent 2σ upper limits for non-detected sources. The solid line is the expected flux density of the starburst galaxy Arp 220 as a function of redshift.

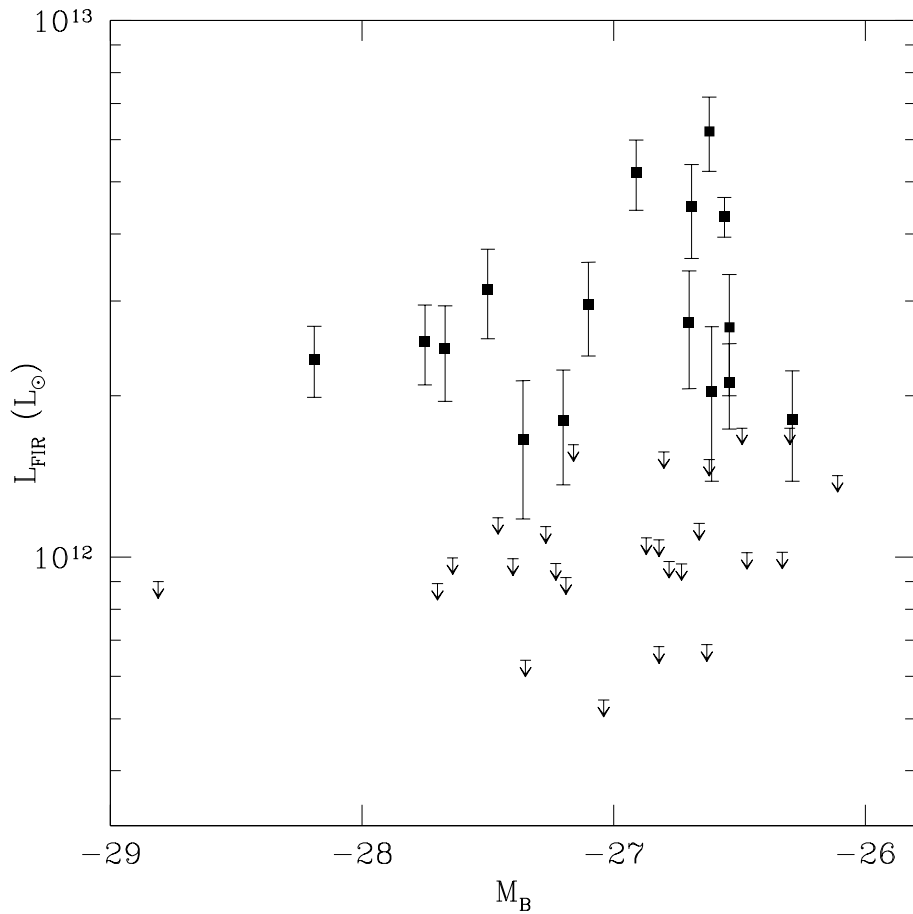


Fig. 2.— The relationship between M_B and L_{FIR} for the SDSS high redshift QSOs listed in Table 1. The symbols are the same as in Figure 1.

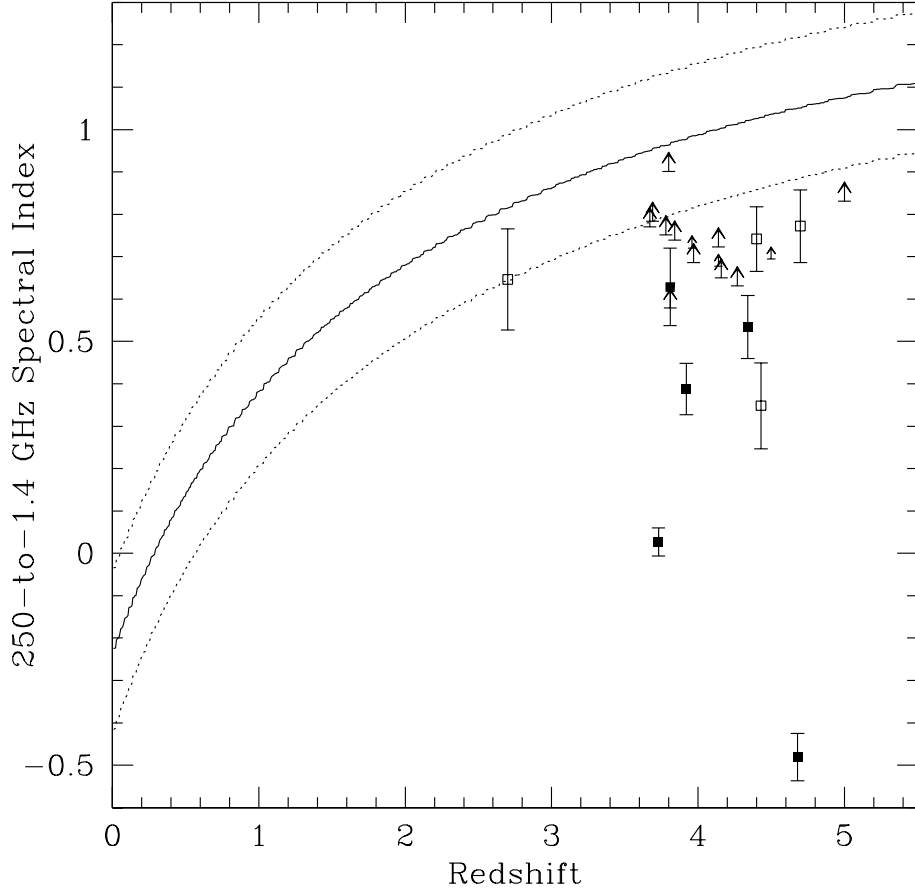


Fig. 3.— The solid curve shows the relationship between redshift and the observed spectral index between 1.4 and 250 GHz for star forming galaxies, as derived from the models presented in Carilli & Yun (2000). The dotted lines show the rms scatter in the distribution. The solid symbols show data for SDSS high redshift QSOs that were detected at 250 GHz. The open symbols are for APM QSOs detected at 250 GHz (Omont et al. 1996a). The squares are for sources detected at 1.4 GHz, while the arrows show lower limits (2σ) to the spectral indices for sources that were not detected at 1.4 GHz. Smaller arrows are for the APM QSOs.

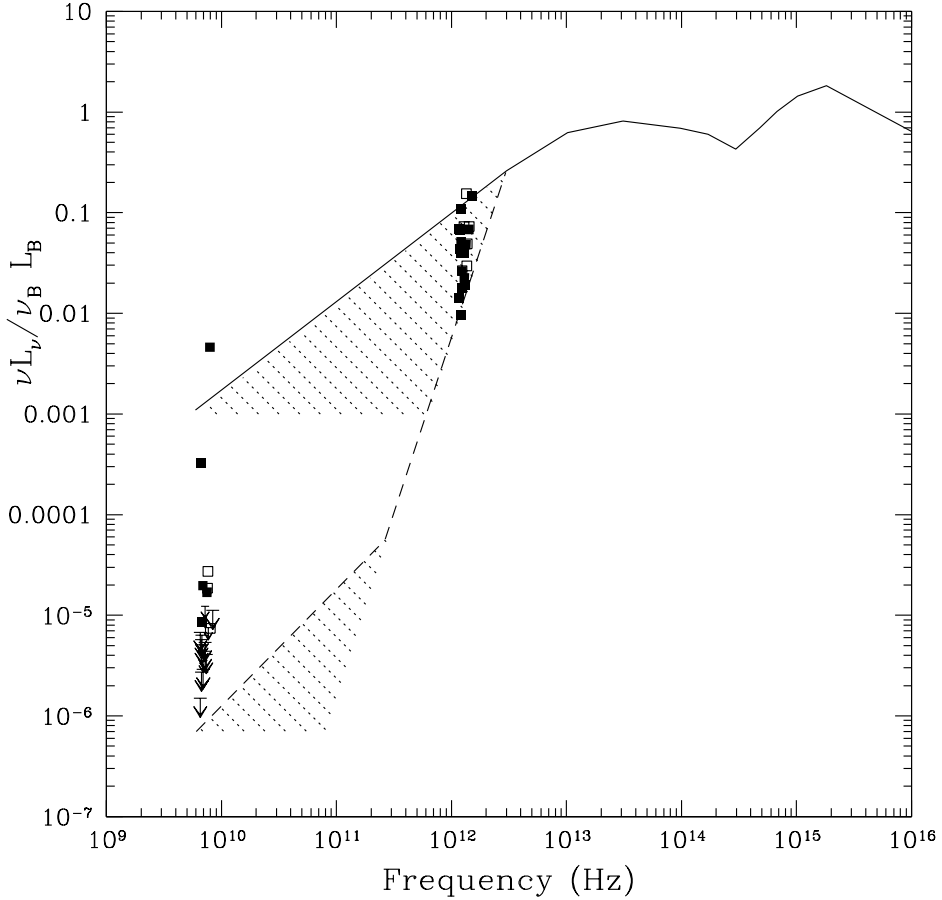


Fig. 4.— The curves show the radio through UV Spectral Energy Distributions (SEDs) for QSOs, taken from Sanders et al. 1989. All data have been normalized to the rest frame blue spectral luminosity. For frequencies above 3×10^{12} Hz, the solid curve shows the mean spectral energy distribution for the PG QSO sample, which is approximately the same for radio-loud and radio-quiet sources. Below 3×10^{12} Hz, the hatched regions show the allowed ranges given the scatter in the observed properties of the PG QSO sample at cm and mm wavelengths, with the solid line delineating the radio-loud sources and the dashed-line the radio quiet sources. The solid symbols show the values derived for the SDSS QSOs detected at 250 GHz as listed in Table 1, while the open symbols are for APM QSOs detected at 250 GHz (Omont et al. 1996a). The arrows show (2 σ) upper limits at 1.4 GHz. The small arrows are for the APM QSOs.